JTTEE5 24:1513–1519
DOI: 10.1007/s11666-015-0348-6
1059-9630/$19.00 © ASM International

Post-treatment of Plasma-Sprayed Cr_2O_3 with Methane-Containing Gas for Conversion to Binder-Free Cr_3C_2

Michael C. Brupbacher, Dajie Zhang, William M. Buchta, Yo-Rhin Rhim, Dennis C. Nagle, and James B. Spicer

(Submitted May 18, 2015; in revised form October 2, 2015)

In most applications, the performance of thermally sprayed Cr_3C_2-NiCr cermet coatings is known to be adversely affected by the presence of the NiCr binder phase. A processing technique for the rapid synthesis of Cr_3C_2 on industrial-scale components could improve the functionality of these coatings by eliminating the metallic binder phase. To form a thick, continuous surface layer of adherent, binder-free Cr_3C_2, the reduction of plasma-sprayed Cr_2O_3 with methane-containing gas was investigated. Conversion of the plasma-sprayed Cr_2O_3 to carbide resulted in a significant increase in coating porosity, yielding a highly microporous Cr_3C_2 surface layer. The physical characteristics of the reduction process appear to be dependent on the coating defect structure at the reduction temperature. Phase morphology and porosity evolution throughout the reduction process were qualitatively examined using x-ray diffraction and scanning electron microscopy. The utility of the resultant Cr_3C_2 coating is discussed with respect to these microstructural characterizations and microindentation hardness measurements.

Keywords atmospheric plasma spray (APS), chromium carbide, oxides

1. Introduction

The reaction mechanisms and the kinetics of the reduction of chromium oxide (Cr_2O_3) powder and pressed pellets with methane-containing gas have been studied extensively, and the body of related work is a testament to the industrial importance of this process (Ref 1-5). Although the details of the proposed reaction mechanisms describing reduction vary, one central notion prevails—namely, a particular phase of chromium carbide, Cr_3C_2, is the end product of complete conversion. Also, there is an agreement on the pronounced effect that methane concentration has on the rate of reduction—above a critical methane concentration, the deposition of carbon can strongly retard Cr_3C_2 formation. In addition, the relatively low temperatures and short reaction times observed by many authors for complete conversion to Cr_3C_2 compared to solid-state carbothermal reduction processing (Ref 6, 7) highlight the usefulness of exploiting a vapor-phase reducing agent. Beyond the production of Cr_3C_2, this material plays a central role as a component in feedstock powder for cermet thermal spray coatings.

In order to facilitate bonding between the feedstock powder and the substrate during spraying, a metallic binder phase (e.g., NiCr) is used for the deposition of Cr_3C_2 via thermal spray techniques such as high-velocity oxy-fuel (HVOF). Significant effort examining the behavior of HVOF Cr_3C_2-NiCr cermet coatings in diverse end-use conditions has shown that the functionalities of these coatings are heavily influenced by the presence of the NiCr binder phase (Ref 8-10). For example, for erosion performance, one of two erosion mechanisms predominately affected the NiCr binder phase, degrading coating integrity in turn (Ref 8). Similarly, hot corrosion in molten oxide salt environments was limited by oxidation of the NiCr binder phase (Ref 9). For tribology applications, the size and the distribution of Cr_3C_2 particles within the NiCr binder phase affected the abrasive wear resistance, suggesting that variations in cohesion between these differing materials contributed to the measured wear rate fluctuations (Ref 10). These characteristics of HVOF Cr_3C_2-NiCr cermet coatings and the deposition requirements for Cr_3C_2 indicate that a carbide coating formation process that takes advantage of thermal spray technologies without requiring the use of an NiCr binder phase could produce coatings with improved performance for a range of applications.

Even though there are many studies concerning the reduction of Cr_2O_3 powder and pressed pellets with methane-containing gas, the synthesis of binder-free Cr_3C_2 coatings via reduction of thermally sprayed Cr_2O_3 appears to be relatively unexplored. In this work, the reduction of atmospheric-plasma-sprayed (APS) Cr_2O_3 with methane-containing gas has been investigated. Plasma-sprayed Cr_2O_3 coatings were exposed to a flowing, methane-con-

Michael C. Brupbacher, Dajie Zhang, and **James B. Spicer**, Department of Materials Science and Engineering, The Johns Hopkins University, 3400 North Charles Street, Baltimore, MD 21218; and **William M. Buchta, Yo-Rhin Rhim,** and **Dennis C. Nagle**, The Johns Hopkins University Applied Physics Laboratory, 11100 Johns Hopkins Road, Laurel, MD 20723. Contact e-mails: mbrupba2@jhu.edu, dzhang9@jhu.edu, mark.buchta@jhuapl.edu, yo-rhin.rhim@jhuapl.edu, dennis.nagle@jhuapl.edu, and spicer@jhu.edu.

taining atmosphere at 1000 °C to isothermally convert the as-deposited oxide to Cr_3C_2. Physical mechanisms of reduction as well as the minimum reaction times required for complete conversion to Cr_3C_2 were investigated using microstructural characterization throughout the reduction process. Measurements were carried out using x-ray diffraction (XRD) and scanning electron microscopy (SEM) to qualitatively examine phase morphology and porosity evolution in the coating. Resultant carbide coating hardness was also determined via microindentation methods for comparison to values reported in the literature for thermally sprayed Cr_3C_2-NiCr cermets.

2. Experimental

2.1 Substrate Materials and Preparation

Due to the temperature range of interest for Cr_2O_3 reduction experiments that exploit methane-containing gas as a reducing agent (800-1200 °C) (Ref 1-5), substrate materials are generally limited to those capable of undergoing short-term, high-temperature exposure without incurring considerable microstructural re-arrangement. These materials include advanced ceramics (e.g., carbon fiber-reinforced carbon) and Ni-based alloys commonly used in high-temperature applications. Since carbon-based materials could act as a supplementary solid-state source of carbon for Cr_2O_3 reduction, an Ni-based alloy substrate was selected for this study—Haynes 230 (H230) (Haynes International, Windsor, Connecticut 06095, USA). The nominal chemical composition of this alloy is shown in Table 1 (Ref 11). Coupons measuring 76.2 × 25.4 × 3.175 mm were machined from a H230 sheet (per AMS 5878C) using waterjet cutting. Surface preparations for plasma spraying involved grit blasting with 36 grit Al_2O_3, followed by cleaning with isopropyl alcohol and compressed air in an effort to remove adherent oxide particles.

Table 1 Nominal chemical composition (wt.%) of H230 alloy

Ni	Cr	W	Mo	Fe	Co	Mn	Si	Al	C	La	B
57	22	14	2	3	5	0.5	0.4	0.3	0.10	0.02	0.015

2.2 Cr_2O_3 Coating Deposition

Owing to the congruent nature by which Cr_2O_3 melts, deposition by means of APS does not require the use of a metallic binder phase (as is the case of incongruently melting Cr_3C_2). However, a bond layer is typically applied between ceramic deposits and metallic substrates to reduce thermal-mismatch stresses that can occur in high-temperature applications. In this work, an NiCr-Al bond layer between the Cr_2O_3 top coat and the H230 substrate was used to moderate cracking and spallation of the oxide coating during heating to the reduction temperature (1000 °C). SEM micrographs of the feedstock powders used in this work are shown in Fig. 1 and their characteristics are provided in Table 2 (Metco, Westbury, NY 11590, USA). An APS system consisting of a 9 MB plasma gun (Metco, Westbury, NY 11590, USA), Model 1200 powder feeder (Bay State Surface Technologies, Auburn, MA 01501, USA), and HP20 robot movement (Yaskawa Motoman, Miamisburg, OH 45342, USA) was used for the deposition of both the NiCr-Al bond layer and the Cr_2O_3 top coat. APS deposition conditions in Ar/H_2 plasma are reported in Table 3.

2.3 Reduction of Plasma-Sprayed Cr_2O_3 with Methane-Containing Gas

Plasma-sprayed Cr_2O_3 coatings were exposed to a flowing, methane-containing atmosphere (80 vol.% Ar with 20 vol.% CH_4; 250 SCCM) in a horizontal quartz tube (60 × 64 × 1300 mm) furnace for 0.1-0.4 h at 1000 °C. The system was purged for 3 h with 400 SCCM Ar prior to the initiation of the thermal cycle. Heating and cooling ramps were carried out at a rate of 400 and 200 °C/h, respectively, with an atmosphere of 200 SCCM Ar. Ultra-high-purity gas sources were used in conjunction with an in-line Nanochem Purifilter (Matheson, Basking Ridge, NJ 07920, USA) to further reduce O_2 and H_2O

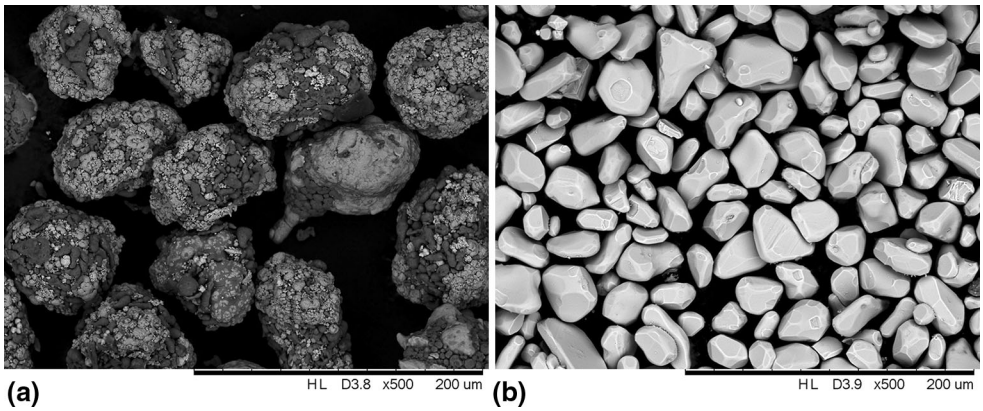

Fig. 1 SEM micrographs of feedstock powder morphologies: (a) NiCr-Al used in the bond layer and (b) Cr_2O_3 used in the top coat

Table 2 Feedstock powder characteristics

Feedstock powder	Chemical composition, wt.%	Particle size, μm	Morphology
Metco 443NS	Ni 18.5Cr 6Al	−125 +45	Spherical
Amdry 6420	99.5 + Cr_2O_3	−45 +22	Irregular

Table 3 Atmospheric plasma spray (APS) deposition conditions in Ar/H_2 plasma

Feedstock powder	Voltage, V	Current, A	Working distance, mm	Traverse speed, mm/s	Step size, mm
Metco 443NS	75	500	127	416.56	3.175
Amdry 6420	70	500	69.85	416.56	3.175

impurity levels (<0.1 ppb O_2 and H_2O). The gas mixture composition was regulated through the use of Series MC mass flow controllers (Alicat Scientific, Tucson, AZ 85743, USA) (Ref 12).

2.4 Microstructural Characterization

2.4.1 Phase Identification. The coating phase evolution throughout the reduction process was determined using x-ray diffraction with an X'Pert Pro Materials Research Diffractometer (Philips, Andover, MA 01810, USA) equipped with a Cu-Kα source. A programmable divergence slit was used to hold the irradiated length constant (8 mm) throughout the scan range, thereby increasing the signal-to-noise ratio for high-angle diffraction peaks.

2.4.2 Metallographic Sample Preparation and SEM. Phase morphology and porosity evolution were qualitatively examined in coating cross sections for various reduction times (0.1-0.4 h) with a TM3000 tabletop SEM (Hitachi, Schaumburg, IL 60173, USA). Samples were initially vacuum-impregnated with EpoThin low-viscosity epoxy (Buehler, Lake Bluff, Illinois 60044, USA) at a pressure of 33.6 kPa. Sectioning, grinding, and polishing were then performed using the recommended techniques for the metallographic preparation of thermally sprayed ceramics (ASTM E1920-03). An IsoMet 1000 low-speed precision diamond saw (Buehler, Lake Bluff, Illinois 60044, USA) and an EcoMet 3000/AutoMet 2000 semi-automatic grinder/polisher (Buehler, Lake Bluff, Illinois 60044, USA) were used for sectioning and grinding/polishing, respectively.

2.4.3 Metallographic Sample Preparation and Microindentation Hardness Testing. Samples for microindentation hardness testing were cross-sectioned in free-standing form and subsequently encapsulated in EpoCure 2 epoxy (Buehler, Lake Bluff, Illinois 60044, USA) without vacuum impregnation. Encapsulation of samples with a relatively high-viscosity epoxy at atmospheric pressure inhibits the impregnation of mounting media into the coating pore structure. Therefore, the measured values reflect the true hardness of the porous coating under investigation. Grinding and polishing procedures followed those implemented in the preparation of coating cross sections for SEM. A series of 10 indentations were made on coating cross sections with an LM100 microindenter (LECO, St. Joseph, MI 49085) and a Vickers indentation tip. Test force (100 gf), indentation spacing (0.635 mm) and dwell time (15 s) were chosen in accordance to the standard test method for Vickers indentation hardness of advanced ceramics (ASTM C1327-08).

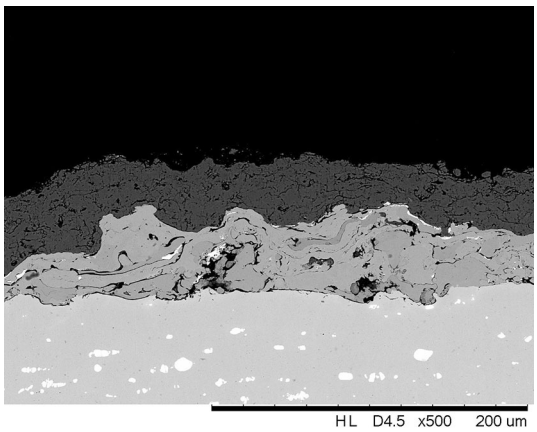

Fig. 2 Cross-sectional SEM micrograph of plasma-sprayed Cr_2O_3 (top coat), showing a complex pore structure containing globular voids, interlamellar porosity, and intralamellar microcracks. Thicker Cr_2O_3 coatings were employed for reduction experiments

3. Results

The aspects of the Cr_2O_3 reduction process are directly related to the characteristics of the as-deposited coating microstructure. XRD measurements of the Cr_2O_3 feedstock powder and the resulting plasma-sprayed coating (Fig. 3) indicate no appreciable compositional changes as a result of the deposition process. Although thicker Cr_2O_3 coatings were employed for reduction experiments, the SEM cross-sectional micrograph shown in Fig. 2 is representative of the plasma-sprayed Cr_2O_3 used in this work. The as-deposited coating microstructure contains globular voids and interlamellar porosity, which are characteristic of a wide range of thermally sprayed materials (Ref 13), as well as the intralamellar microcracks that occur in brittle ceramics (Ref 14).

Despite uncertainty regarding the reaction mechanisms of reduction of Cr_2O_3 powder and pressed pellets with

methane-containing gas, there is an agreement that the conversion to Cr_3C_2 largely proceeds by the following overall chemical equation (Ref 1-5):

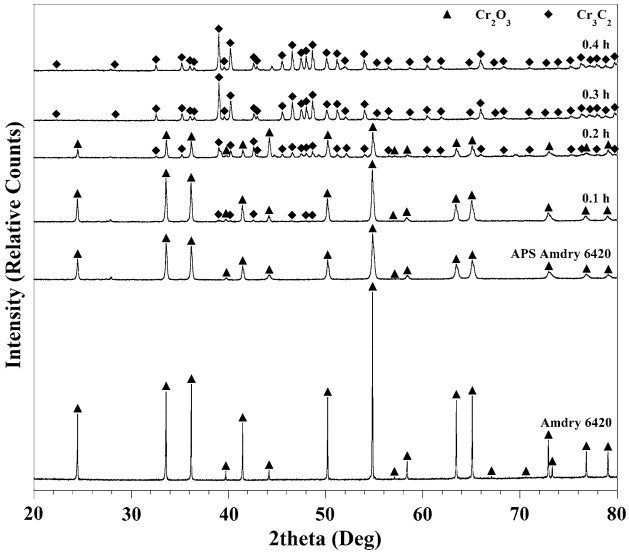

Fig. 3 XRD patterns of plasma-sprayed Cr_2O_3 after various reduction times (0.1-0.4 h) at 1000 °C, showing coating phase evolution from Cr_2O_3 to binder-free Cr_3C_2

$$3Cr_2O_{3(s)} + 13CH_{4(g)} \rightarrow 2Cr_3C_{2(s)} + 9CO_{(g)} + 26H_{2(g)}. \quad \text{(Eq 1)}$$

In this work, it was found that the complete conversion of plasma-sprayed Cr_2O_3 to Cr_3C_2 occurred over timescales similar to those reported in related work which exploited vapor-phase reducing agents (Ref 1-5), but differed significantly from those reported for solid-state carbothermal reduction investigations (Ref 6, 7). The XRD patterns in Fig. 3 show the coating phase evolution for reduction times of 0.1-0.4 h at 1000 °C.

For a reduction time of 0.1 h, the onset of Cr_3C_2 formation is observable while Cr_2O_3 clearly remains the major phase in the coating. With increased reduction time (0.2 h), a substantial volume fraction of the Cr_2O_3 coating is converted to Cr_3C_2. After a reduction time of 0.3 h, the conversion to Cr_3C_2 is complete (to the penetration depth of the x-ray beam), and an XRD pattern with relative intensities closely matching randomly oriented, polycrystalline Cr_3C_2 is achieved (Ref 15). An extended reduction time of 0.4 h however produces no appreciable compositional change in the carbide coating. These measurements demonstrate the ability to form binder-free Cr_3C_2 coatings via reduction of plasma-sprayed Cr_2O_3 with methane-containing gas—this is one of the principal results of this work. Previous investigation has shown that the initial porosity in sprayed Cr coatings affects the carburization

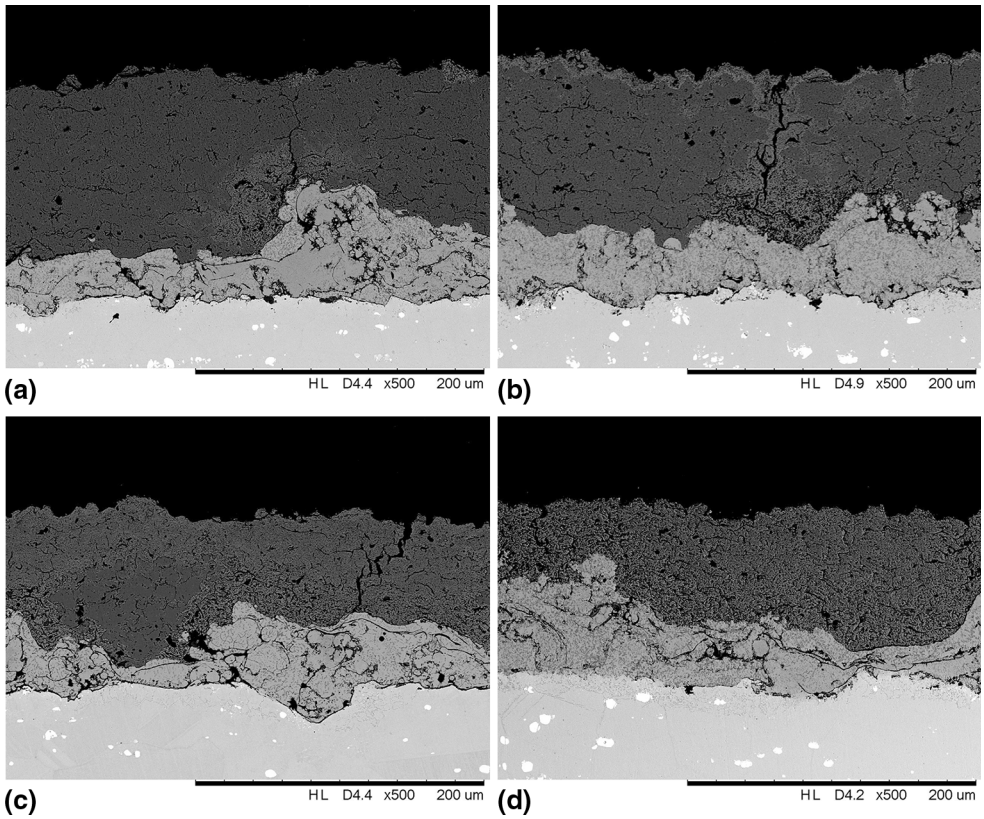

Fig. 4 Cross-sectional SEM micrographs of plasma-sprayed Cr_2O_3 after various reduction times at 1000 °C, illustrating characteristics of the physical mechanism of reduction to binder-free Cr_3C_2: (a) 0.1 h, (b) 0.2 h, (c) 0.3 h, and (d) 0.4 h

process (Ref 16), and it is conceivable that defects in plasma-sprayed Cr_2O_3 could serve a similar role in achieving through-thickness conversion. The SEM micrographs in Fig. 4 show the coating phase morphology and porosity evolution throughout the reduction process, and illustrate characteristics of the physical mechanism of reduction with methane-containing gas when employing a plasma-sprayed coating precursor.

At the earliest reduction time (0.1 h), the onset of Cr_3C_2 formation (visible in areas of increased image brightness relative to the surrounding unconverted Cr_2O_3) appears to be limited to the near-surface region of the coating and to areas containing sizeable microcracks oriented normal to the plane of the coating (Fig. 4a). Considering that the out-of-plane dimensions of these microcracks far exceed splat thicknesses and also that they were not present in the as-deposited Cr_2O_3 coating microstructure (Fig. 2), it is likely that they result from thermal-mismatch stresses generated by heating to the reduction temperature (1000 °C) (Ref 13, 14). Even though the NiCr-Al bond layer did not prevent microcracking, the enhanced rate of reduction in the vicinity of microcracks indicates that defects in plasma-sprayed Cr_2O_3 facilitate through-thickness conversion. Inspection of Fig. 4(b) for a reduction time of 0.2 h further suggests that multiple pathways for reduction are acting. While reduction seems to proceed in plane by means of thermal-stress-generated microcracks, carbide formation also occurs progressively from the surface to underlying unconverted Cr_2O_3 in other areas of the coating microstructure. Although the imaging results for a reduction time of 0.3 h (Fig. 4c) agree with the XRD measurements presented in Fig. 3 (the Cr_3C_2 surface layer thickness exceeds the x-ray beam penetration depth), an underlying portion of oxide remains unconverted in regions of increased Cr_2O_3 thickness. In areas of the microstructure containing thermal-stress-generated microcracks, carbide formation has progressed through the coating thickness. Closer examination of the interface between the Cr_3C_2 surface layer and the underlying unconverted Cr_2O_3 in Fig. 4(c) reveals a significant difference in porosity between the two phases, as well as preferential carbide formation along Cr_2O_3 grain boundaries (Fig. 5). Void formation of similar character has been documented in previous work involving the conversion of Cr_2O_3 powder to Cr_3C_2 via reduction with methane-containing gas (Ref 1); however, in this particular instance it is probable that the newly formed microporous Cr_3C_2 is a combined result of the constraint on coating dimensions imposed by the substrate and the specific volume decrease associated with Eq 1 (38.1%). After 0.4 h of reduction (Fig. 4d), carbide formation has advanced through the coating thickness along the entirety of the cross section under observation. Irrespective of the coating location under consideration, a thick, continuous surface layer of adherent, binder-free Cr_3C_2 is formed after a reduction time of 0.3 h.

Microindentation hardness testing has been performed on the binder-free Cr_3C_2 coating cross section resulting from 0.4 h of reduction, and the results are summarized in Table 4. The measured average hardness for indentations that passed

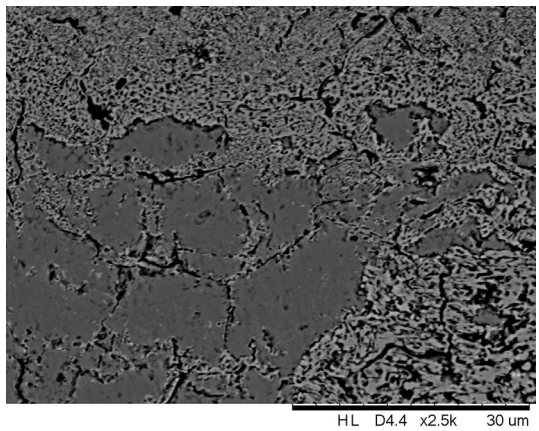

Fig. 5 Void formation in the Cr_3C_2 phase formed from the reduction of plasma-sprayed Cr_2O_3

the acceptability criteria outlined in ASTM C1327-08 (344 HV_{100}) is well below what has been reported for conventional and nanostructured Cr_3C_2-NiCr cermet coatings (Ref 17), though this result likely reflects the diminished hardness of a highly microporous, binder-free Cr_3C_2 coating relative to the fully dense, pure carbide. Indentations with unacceptable deviations in measured diagonal lengths arose from intersection of the indentation tip and the coating defect structure. Based on these observations, improvements to the reduction process should focus on manipulation of the as-deposited Cr_2O_3 coating microstructure to yield nanoporous, binder-free Cr_3C_2 coatings. Unlike the coatings reported in this work, nanoporous carbide coatings could provide near-theoretical hardness.

4. Discussion

Although thermogravimetric or on-line off-gas mass spectroscopy techniques will be needed to quantify the reaction kinetics of the reduction of plasma-sprayed Cr_2O_3 with methane-containing gas (Ref 1, 2, 5), a qualitative understanding can be gained from the XRD and SEM results presented in Fig. 3 and 4. Since non-catalytic gas-solid reactions are inherently multi-step phenomena, both chemical and physical (diffusional) processes must be considered when identifying the rate-limiting step in the overall reaction (Ref 18, 19). The lack of diffraction peaks belonging to carbon in the XRD patterns for all of the reduction times in this work (Fig. 3) suggests the newly formed microporous Cr_3C_2 is a non-catalytic surface for methane decomposition. Also, this lack of carbon deposition indicates that the diffusion of reducing agents rather than their chemical reactivity is probably the rate-limiting step in the overall reaction. This notion contrasts with previous modeling involving the reaction kinetics of the reduction of pressed Cr_2O_3 pellets with methane-containing gas (Ref 2), which operated under the assumption that chemical reactivity was the rate-limiting step. However, the low-density pressed pellets in preceding studies

Table 4 Microindentation hardness testing report

Number of indentations	Number of acceptable indentations	Dwell time, s	Indentation spacing, mm	Average hardness (HV_{100})	Standard deviation (HV_{100})
10	8	15	0.635	344.75	30.38

were formed from an initially porous Cr_2O_3 powder which likely resulted in a physical system that supported such a model. Regardless of the rate-limiting step under consideration, the progression of conversion over time (Fig. 4) seems to indicate that the overall reaction extent is nonlinear in nature when employing a plasma-sprayed Cr_2O_3 coating precursor. This is in agreement with previous work using Cr_2O_3 powder and pressed pellets, which quantified the extent of overall reactions under isothermal conditions (Ref 1, 5). In addition, the timescale over which complete conversion occurs (less than 0.5 h) compares favorably with these previous reports—this was unexpected considering the large differences in density between the powder, pressed pellet, and plasma-sprayed Cr_2O_3 preforms.

Also of significance is the disparity between the timescales required for the complete conversion of plasma-sprayed Cr and Cr_2O_3 to Cr_3C_2 under identical conditions. In this work, the complete conversion of plasma-sprayed Cr_2O_3 to Cr_3C_2 is realized in less than 0.5 h, whereas previous investigation involving the carburization of plasma-sprayed Cr suggested that complete conversion required at least several hours (Ref 16). A fundamental difference in the physical mechanism of conversion is probably responsible for this discrepancy. While microcracking in the Cr_2O_3 coating defect structure facilitates rapid through-thickness reducing agent penetration, subsequent transport is likely occurring by means of methane gas diffusion through microporosity in the newly formed Cr_3C_2 in order to reach unconverted oxide. Specific models will be needed to confirm a self-assisted physical conversion mechanism of this nature.

Defects such as microcracks and microporosity are ordinarily considered to be detrimental microstructural features in industrially important carbide coating applications—including those that require wear-corrosion resistance. However, the defect-ridden Cr_3C_2 coatings produced in this work could serve as refractory scaffoldings for the formation of multi-functional coatings. Owing to the high level of microporosity, as well as the relatively uniform pore size and spatial distribution, the pore structure of such refractory-carbide scaffoldings could be filled with materials possessing desirable application-oriented properties. Furthermore, refractory carbides are well known to exhibit low chemical reactivity at high temperatures. As a result of these characteristics, refractory-carbide scaffoldings could be impregnated with a range of materials, providing a variety of potential multifunctional, impermeable protective coatings. For example, pores could be filled with various polymers to yield wear-resistant, sealed coatings for low-temperature applications, while liquid metal infiltration could produce coatings for use at significantly higher temperatures (Ref 20).

The expeditious conversion of plasma-sprayed Cr_2O_3 to Cr_3C_2 may point toward directions for the rapid synthesis of other binder-free refractory carbide coatings of industrial importance, such as tungsten carbide (WC). The conversion of tungsten oxide (WO_3) powder to WC via reduction with methane-containing gas has been shown to result in an increase in particle porosity (Ref 21); therefore, it is likely that plasma-sprayed WO_3 would follow a physical reduction mechanism similar to what has been observed in the instance of plasma-sprayed Cr_2O_3. Future efforts should involve investigating the ability to convert the remaining group IV-VI refractory oxides to binder-free carbide in order to further substantiate the significance of this processing technique.

5. Conclusion

In this work, a method has been demonstrated for the synthesis of binder-free Cr_3C_2 coatings on nickel-based alloys via the reduction of plasma-sprayed Cr_2O_3 with methane-containing gas. A thick, continuous surface layer of adherent, binder-free Cr_3C_2 has been achieved, with the physical mechanism of reduction being strongly influenced by the coating defect structure at the reduction temperature. Despite large differences in density between oxide preforms, the conversion of plasma-sprayed Cr_2O_3 to Cr_3C_2 reported here occurs over timescales similar to those in related work that used Cr_2O_3 power and pressed pellets. This might be due in part to the formation of microporosity in the newly formed Cr_3C_2, which appears to expedite the diffusion of methane gas to unconverted Cr_2O_3. Beyond playing a significant role in the physical mechanism of reduction, microporous Cr_3C_2 could serve as a refractory scaffolding for use in the development of multi-functional coatings.

Acknowledgment

The authors gratefully acknowledge the support of the U.S. Department of Energy (DOE) through the Nuclear Energy University Program (NEUP) Contract No. 101630.

References

1. N. Anacleto and O. Ostrovski, Solid-State Reduction of Chromium Oxide by Methane-Containing Gas, *Metall. Mater. Trans. B*, 2004, **35B**(4), p 609-615
2. P.J. Read, D.A. Reeve, J.H. Walsh, and J.E. Rehder, Reduction of Chromites in Methane-Hydrogen Mixtures-Chromium Sesquioxide, *Can. Metall. Q.*, 1974, **13**(4), p 587-595

3. M.A. Qayyum and D.A. Reeve, Reduction of Chromites to Sponge Ferrochromium in Methane-Hydrogen Mixtures, *Can. Metall. Q.*, 1976, **15**(3), p 193-200
4. R. Ebrahimi-Kahrizsangi, H. Monajati Zadeh, and V. Nemati, Synthesis of Chromium Carbide by Reduction of Chromium Oxide with Methane, *Int. J. Refract. Met. Hard Mater.*, 2010, **28**(3), p 412-415
5. B. Khoshandam, R.V. Kumar, and E. Jamshidi, Producing Chromium Carbide Using Reduction of Chromium Oxide with Methane, *Am. Inst. Chem. Eng. J.*, 2006, **52**(3), p 1094-1102
6. L.-M. Berger, S. Stolle, W. Gruner, and K. Wetzig, Investigation of the Carbothermal Reduction Process of Chromium Oxide by Micro- and Lab-Scale Methods, *Int. J. Refract. Met. Hard Mater.*, 2001, **19**(2), p 109-121
7. W. Gruner, S. Stolle, and K. Wetzig, Formation of CO_x Species During the Carbothermal Reduction of Oxides of Zr, Si, Ti, Cr, W, and Mo, *Int. J. Refract. Met. Hard. Mater.*, 2000, **18**(2-3), p 137-145
8. G.-C. Ji, C.-J. Li, Y.-Y. Wang, and W.-Y. Li, Erosion Performance of HVOF-Sprayed Cr_3C_2 NiCr Coatings, *J. Therm. Spray Technol.*, 2007, **16**(4), p 557-565
9. T.S. Sidhu, S. Prakash, and R.D. Agrawal, Characterizations and Hot Corrosion Resistance of Cr_3C_2-NiCr Coating on Ni-base Superalloys in an Aggressive Environment, *J. Therm. Spray Technol.*, 2006, **15**(4), p 811-816
10. G. Matthäus, J.A. Picas, and A. Forn, Effect of Feedstock Powder Size on the Sliding Wear Behavior of Thermal Sprayed HVOF Cr_3C_2-NiCr Coatings. Thermal Spray 2004: Advances in Technology and Application, *Proceedings of the International Thermal Spray Conference*, 2004. ASM International, May 10-12, 2004 (Osaka, Japan), ASM International, 2004, p 529-533
11. http://www.haynesintl.com/pdf/h3000.pdf, 2015
12. M.C. Brupbacher, D. Zhang, W.M. Buchta, J.B. Spicer, and D.C. Nagle, *Formation of Molten Fluoride Salt Corrosion Resistant Coatings on Nickel-Based Alloys, ANS Transactions*, Vol. 111, (Anaheim, CA), ANS, 2014, p 584-587
13. C.-J. Li and A. Ohmori, Relationship Between the Microstructure and Properties of Thermally Sprayed Deposits, *J. Therm. Spray Technol.*, 2002, **11**(3), p 365-374
14. S. Kuroda and T.W. Clyne, The Quenching Stress in Thermally Sprayed Coatings, *Thin Solid Films*, 1991, **200**(1), p 49-66
15. S. Rundqvist and G. Runnsjö, Crystal Structure Refinement of Cr_3C_2, *Acta Chem. Scand.*, 1969, **23**(4), p 1191-1199
16. M.C. Brupbacher, D. Zhang, W.M. Buchta, M.L. Graybeal, Y.-R. Rhim, D.C. Nagle, and J.B. Spicer, Synthesis and Characterization of Binder-Free Cr_3C_2 Coatings on Nickel-Based Alloys for Molten Fluoride Salt Corrosion Resistance, *J. Nucl. Mater.*, 2015, **461**, p 215-220
17. J. He, M. Ice, and E.J. Lavernia, Synthesis of Nanostructured Cr_3C_2-25(Ni20Cr) Coatings, *Metall. Mater. Trans. A*, 2000, **31A**(2), p 555-564
18. J.J. Carberry, *Fluid-Solid Noncatalytic Reactions, Chemical and Catalytic Reaction Engineering*, General Publishing Company, Ltd, Toronto, Ontario, 2001, p 310-356
19. P.A. Ramachandran and L.K. Doraiswamy, Modeling of Noncatalytic Gas-Solid Reactions, *Am. Inst. Chem. Eng. J.*, 1982, **28**(6), p 881-900
20. J. Knuuttila, P. Sorsa, and T. Mäntylä, Sealing of Thermal Spray Coatings by Impregnation, *J. Therm. Spray Technol.*, 1999, **8**(2), p 249-257
21. F.F.P. Medeiros, S.A. De Oliveira, C.P. De Souza, A.G.P. Da Silva, U.U. Gomes, and J.F. De Souza, Synthesis of Tungsten Carbide through Gas-Solid Reaction at Low Temperatures, *Mater. Sci. Eng. A*, 2001, **315**(1-2), p 58-62